# Putting Together the Puzzle of Ion Transfer in Single-Digit Carbon Nanotubes: Mean-Field Meets Ab Initio

| | |
|---|---|
| Journal: | *Nanoscale* |
| Manuscript ID | NR-ART-12-2021-008073.R1 |
| Article Type: | Paper |
| Date Submitted by the Author: | 05-Apr-2022 |
| Complete List of Authors: | Neklyudov, Vadim; Technion Israel Institute of Technology, The Wolfson Department of Chemical Engineering<br>Freger, Viatcheslav ; Technion Israel Institute of Technology, The Wolfson Department of Chemical Engineering |
| | |

# Putting Together the Puzzle of Ion Transfer in Single-Digit Carbon Nanotubes: Mean-Field Meets Ab Initio

Vadim Neklyudov[†] and Viatcheslav Freger[*,†,‡,¶]

[†] *Wolfson Department of Chemical Engineering, Technion - IIT, Haifa 32000, Israel*

[‡] *Russel Berrie Nanotechnology Institute, Technion - IIT, Haifa 32000, Israel*

[¶] *Grand Technion Energy Program, Technion - IIT, Haifa 32000, Israel*

E-mail: vfreger@technion.ac.il

Phone: +972 (0) 4 829 2933

**Abstract**

Nature employs channel proteins to selectively pass water across cell membranes, which inspires search for bio-mimetic analogues. Carbon nanotube porins (CNTPs) are intriguing mimics of water channels, yet ion transport in CNTPs still poses questions. As alternative to continuum models, here we present a molecular mean-field model that transparently describes ion coupling, yet unlike continuum models, computes *ab initio* all required thermodynamic quantities for KCl salt and $H^+$ and $OH^-$ ions present in water. Starting from water transfer, the model considers transfer of free ions, along with ion-pair formation as a proxy of non-mean-field ion-ion interactions. High affinity to hydroxide, suggested by experiments and making it dominant charge carrier in CNTP, is revealed as an exceptionally favorable transfer of KOH pairs. Nevertheless, free ions, coexisting with less mobile ion-pairs, apparently control ion transport. The model explains well the observed effects of salt concentration and pH on conductivity, transport numbers, anion permeation and its activation energies, and current rectification. The proposed approach is extendable to other sub-nanochannels and help design novel osmotic materials and devices.

The world faces a water stress, which is predicted to increase and spread to areas not experiencing the shortage of fresh water today.[1] Production of fresh water via desalination of sea, brackish, and waste water is a viable solution, yet currently used membrane desalination technology still leaves room for improvement and selectivity-tailoring. This motivates research that looks into alternative materials with improved water-salt and ion-ion selectivity.[2] Natural membrane proteins aquaporins efficiently separate water from ions by forcing it through a short and narrow channel in a single-file arrangement at rates exceeding $10^9$ water molecules per second with nearly ideal water-ion selectivity.[3] Intriguingly, while the use of degradable aquaporins might be impractical, stable nanomaterials, such as atomically thin nanoporous nanosheets[4–7] or narrow nanotubes,[8–10] that can mimic transport in aquaporins and offer an exciting next-generation alternative to currently used polymeric membranes.[11,12]

Single-digit carbon nanotube porins (CNTP) share many unique features of aquaporins and demonstrated a water-salt selectivity of $10^5$, commensurate with selectivity of polyamide desalination membranes, the industrial benchmark.[13–15] Numerous theoretical[16–24] and experimental[25–29] studies indicate that, due to wall roughness smaller than the de Brogli length, water transport in CNTPs narrower than about 1.5 nm and similarly narrow graphene slits, occurs in a scatter-less manner, at rates greatly exceeding hydrodynamic predictions[9,30,31] and even faster than water permeation in aquaporins.[22,25] However, while there is an overall consensus regarding water transport in narrow CNTs, the physical mechanisms behind ion rejection still pose many questions. For instance, it has been long believed that negative carboxylic charges at CNTP rims control salt rejection,[32–34] yet recent data on pH dependence of anion permeation downplayed this mechanism. Adsorption of $OH^-$ ions was proposed as an alternative charging mechanism in CNTs and a number of continuum-type nanofluidic models, solving Poisson-Boltzmann and Navier-Stokes equation employed this and other ad hoc assumptions to describe transport, charge formation and conduction in narrow and wide CNTPs and rationalize the observed trends.[27,35–41] In parallel, important insights to transport of ions at the molecular level were obtained using molecular dynamics (MD)[42–45] and *ab initio* computations.[13,46]

The data on ion permeation in CNTPs have mainly come from two types of measurements (a) ion permeation from stop-flow experiments with CNTP-loaded vesicles and (b) conductance or current-voltage (I-V) measurements for CNTPs connecting two solutions across a nanopore. These experiments yielded absolute values of permeabilities to different ions and salts, conductivity and water-salt selectivity for various types of CNTPs and longer tubes. They also determined trends that describe dependence of transport properties on salt concentration and pH, as well as temperature dependence, from which appropriate activation energies could be derived. These trends are often highly characteristic and may serve as fingerprints of physical mechanisms. The data, combined with simulations, e.g., using classical MD[42–45] and *ab initio* computations[13,46] have significantly advanced understanding of ion transport in CNTPs, yet a full and physically consistent picture unifying different experimental findings is still missing.

Here, we develop a systematic molecular picture that transparently describes ion transfer in CNTPs in a hybrid approach. As an alternative to common continuum nanofluidic models, the present models similarly accounts for ion coupling using analytical mean-field relations, yet employs *ab initio* computations rather than classical electrokinetic relations to evaluate quantities pertaining to ion transfer in narrow channels of molecular width. Since KCl has been the salt most often used in experimental studies, we focus on $K^+$ and $Cl^-$ ions, adding to the picture the $OH^-$ and $H^+$ ions inherently present in water. We focus on (6,6) CNTP of diameter 0.8 nm, used in most experiments as benchmark sub-nanometer ("single-digit") channels but, in order to clarify the effect of CNTP diameter and water arrangement, compare the results with narrower (5,5) channels, in which a single-file arrangement is preserved. Importantly, we also consider the effect of the medium surrounding CNTP that was shown to strongly affect ion transfer from a solution to CNTPs.[47] We first incorporate the computed thermodynamic values in a model considering only free ions, retaining their full translational freedom, which is shown to agree semi-quantitatively with most experimental results. Subsequently, we add to the picture formation of ion pairs, as a proxy of non-mean-field ion-ion-CNTP interactions, which removes most remaining inconsistencies. The resulting physical picture rationalizes most results on ion permeation, selectivity, conductance, and current rectification in CNTPs reported so far.

## Internal arrangement of water and ion hydration: not necessarily a single file

The narrowest experimentally studied CNTPs, showing the largest water-ion selectivity, have been the (6,6) nanotubes. Classical MD simulations suggested that water in (6,6) tubes forms a single file, similar to (5,5) nanotubes, believed to be the narrowest ones that allow water and ion transport.[16,40,48,49] Ions in (5,5) tubes are then solvated by only two adjacent water molecules, which is confirmed by computations.[47] The low density of water in a single file and resulting high entropy were suggested[50] to be an important factor in experimentally confirmed spontaneous filling of CNTPs with water.[51] However, *ab initio* simulations recently indicated a possibility of a significantly distorted arrangement in (6,6) CNTPs, both in presence and absence of ions. For instance, while larger $K^+$ ions were still solvated by two water molecules, smaller $Na^+$ cations displayed a four-molecule solvation.[52] Here, we find that significantly distorted arrangements in (6,6) tubes are likely even without ions.

Figure 1a displays two arrangements of water molecules within (6,6) CNTP, composed of a central water molecule surrounded by three other molecules on each side. Corresponding thermodynamic quantities computed by comparing CNTPs containing six and seven water molecules for each arrangement (see Methods) are shown in Fig. 1b. Fairly similar values are computed for (5,5) tubes (see Supplementary Information). We find that, upon energy optimization, the straight file in (6,6) tubes transforms to a zigzag arrangement shown on top of Fig. 1a. The latter has a lower energy yet still preserves the topology of the single file, as each water molecule still interacts with only two closest neighbors. However, upon energy optimization from some other initial arrangements, commensurate energies were obtained for a topologically different arrangement at the bottom of Fig. 1a, with middle molecules bonded to three neighbors. Its energy was ∼10 kJ/mol lower than zigzag's for six water molecules, but similarly higher for seven molecules. We trace this back to the "surface" energy of the file termini, which have the same structure for 6- and 7-member zigzags but are quite different for triple-bonded counterparts due to seventh "under-bonded" terminal molecule. The terminal energy then cancels out in the computed water transfer energy for zigzag but may overestimate the cost of water transfer to the triple-bonded state, which might otherwise yield a transfer energy closer to zigzag's. For this reason, while computing ion transfer energies, we minimize this uncertainty by choosing as a reference precursor state in eqs. 9 and 10 the 6-water file with (terminal) arrangement closest to one obtained around the specific ion.

Since CNTP is an open system, the water equilibrium should minimize the free energy rather than energy. We then computed for each arrangement all thermodynamic functions of water transfer, including excess transfer entropy $\Delta S^{ex}$, excess Gibbs energy $\Delta G^{ex}$ (shown in Fig. 1b), and enthalpy $\Delta H = \Delta G^{ex} + T\Delta S^{ex}$, using Gaussian's thermochemical package. Since water in CNTP is a phase co-existing with water bulk phase, in the manner of Clapeyron equation, the equilibrium requires $\Delta G^{ex} = 0$. While $\Delta S^{ex}$ indicates whether a water arrangement in CNTP is more constrained than the bulk, $\Delta G^{ex}$ indicates how it compares with the equilibrium state. We focus on $\epsilon = 2$, as most representative of CNTPs embedded in the lipid membrane, but the numbers vary weakly with $\epsilon$, since water is not charged (cf. values of ions below), see Fig. 1b.[47] The negative $-T\Delta S^{ex} = -0.8$ kJ/mol of the zigzag arrangement indicates it is slightly less constrained (rarer) than bulk water, whereas its negative $\Delta G^{ex} = -17.3$ kJ/mol indicates it is also rarer than the equilibrium one (open bars in Fig. 1b), i.e., more water is to be inserted to reach equilibrium. On the other hand, the triple-bonded arrangement has a positive $-T\Delta S^{ex} = 3.6$ kJ/mol, i.e., is denser than bulk water. Its positive $\Delta G^{ex} = 19.7$ kJ/mol indicates it is also denser than the equilibrium state, i.e., some water needs to be expelled for reaching equilibrium (cross-hatched bars in Fig. 1b). If $\Delta G^{ex}$ is an overestimate, this arrangement is probably closer to equilibrium than the last number suggests. Nevertheless, the equilibrium arrangement in (6,6) tubes is likely to be intermediate to the zigzag and triple-bonded states, neither of which is a regular single file. Its thermodynamic properties may, in principle, be obtained by full quantum MD simulations on much larger systems but, unfortunately, fast *ab initio* methods suitable for MD, such as pseudopotential-based, poorly estimate bulk hydration,[46] critical in the present context. On the other hand, the computational costs of MD at higher level of theory, such as the one used here, would be formidable.

However, we may estimate the equilibrium properties by appropriately interpolating between the two arrangements. Approximating equilibrium as a superposition of the two states, each weighed by the Boltzmann factor with respective $\Delta G^{ex}$, fractions of each state are found by requiring total $\Delta G^{ex} = 0$. The transfer enthalpy will then be effectively dictated by the state with lower $\Delta G^{ex}$, but only a small fraction of water will be found in this arrangement (see Supplementary Information). While diffusing along CNTP, water will have to assume temporarily the higher energy state. We then speculate that the triple-bonded state may represent the relevant diffusion transition state, whose enthalpy is larger by 15-20 kJ/mol than bulk water. Indeed, Li et al. reported recently a reasonably close experimental activation energy 20 kJ/mol for water permeation through (6,6) CNTPs.[13]

Weaker steric constrains in (6,6) tubes, compared with (5,5), also allow distortions of water arrangement around ions. Thus, the lowest energy straight-file two-molecule hydration of $OH^-$ and $Cl^-$ anions in (5,5) CNTPs,[47] transforms upon optimization to a different, four-molecule hydration with a lower energy within (6,6) CNTP, as shown in Figs. 1c and d. This might partly be due to repulsive interaction of anions with CNT walls, thereby anions tend to assume a position near the CNT main axis, which makes them sterically more accessible for hydration (see Fig. S4d in Supplementary Information). In contrast, cations show a far more attractive interaction with CNT walls and thus tend to assume an eccentric position (Fig. S4c), sterically less accessible for hydration. Then, in agreement with other reports,[52] two-molecule hydration was found here for $K^+$ and $H^+$ (essentially, $H_3O^+$) cations (Figs. 1e and f). Since the energy of internal hydration is a considerable part of the total ion transfer energy, e.g., about 50 % for $K^+$ and 25 % for $Cl^-$ in (5,5) tubes,[47] this difference may affect the energy of ion transfer from water to CNTP. Nevertheless, unlike the case of CNT(5,5),[47] electron-density maps in Fig. S4 show a negligible overlap between the $\pi$-electrons of CNT(6,6) and electron clouds of water or ions. This suggests that the interaction between the $\pi$-electron system of CNTP and ions is mainly electrostatic, favorable for the cations ion and unfavorable for anions.

## How much does it cost to transfer ions?

Figures 1e and f illustrate the ion transfer process and display the key transfer quantities, excess Gibbs energy $\Delta G^{ex}$ and enthalpy $\Delta H$, for moving ions into a water-filled (6,6) CNTP. (Complete data and comparison with (5,5) tubes are presented in Supplementary Information Figs S3.) These quantities are plotted versus $1/\epsilon$ and the slope highlights the contribution by the dielectric energy, i.e., polarization of the medium surrounding CNTP,[47] which adds a significant cost to ion transfer. It reaches a maximum in vacuum ($\epsilon = 1$) and vanishes when $\epsilon$ goes to infinity, i.e., at $1/\epsilon = 0$. Neither of these extremes reflect typical experimental conditions, yet $\epsilon = 2$ ($1/\epsilon = 0.5$) may reasonably represent lipid membranes[53] embedding CNTPs in most experiments. The slopes for the anions are somewhat smaller than for cations. This may be a result of more favorable electrostatic interaction of cations with the CNTP electron cloud and charge redistribution, decreasing the dielectric energy.[47] Yet, the slopes of all ions are reasonably close and similar to results for (5,5) CNTPs (Supplementary Information Fig. S3). This contribution is then about rigidly shifts $\Delta G^{ex}$ and $\Delta H^{ex}$ of all

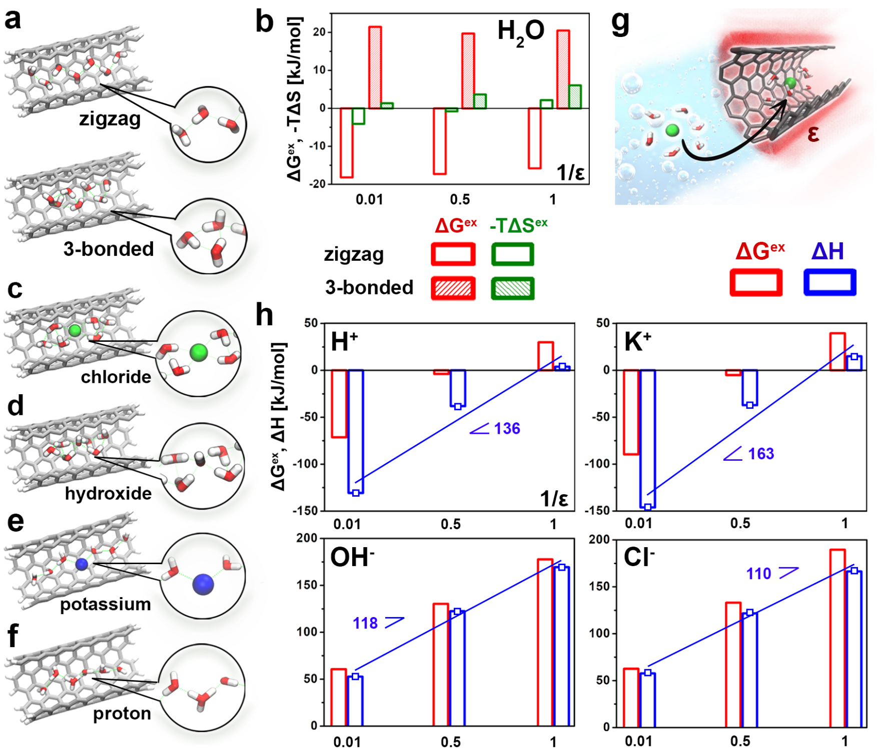

Figure 1: **Molecular arrangement and transfer quantities for water and ions in (6,6) CNTP**. (**a**) Zigzag (top) and triple-bonded (bottom) arrangement of water in CNTP and (**b**) computed $\Delta G^{ex}$ and $-T\Delta S^{ex}$ for water transfer to CNTP for each arrangement at different $\epsilon$. Water arrangement around chloride (**c**), hydroxide (**d**), potassium (**e**) and proton (**f**) ions in water-filled CNTP. (**g**) Schematic illustration of single ion transfer process from bulk water to water-filled CNTP and (**h**) computed transfer quantities, $\Delta G^{ex}$ and $\Delta H$, for transfer of $H^+$, $K^+$, $OH^-$, and $Cl^-$ as single ions plotted versus $1/\epsilon$. The sloped line and the value of the slope highlight the effect of dielectric energy. Oxygen, carbon, and hydrogen atoms and chloride ions are depicted in red, grey, white and green, respectively.

ions relative to ion-specific base values.

Compared to its effect on water transfer, $\Delta S^{ex}$ seems to play a lesser role in ion transfer, therefore $\Delta G^{ex}$ is mainly controlled by enthalpy. Due to more favorable interaction with CNTP, cations have a significantly lower transfer energy than anions. For instance, for $\epsilon = 2$, $K^+$ transfer into CNTP is nearly athermal and, for (6,6) tubes, it is even more favorable than transfer of water, while transfer of anions is highly unfavorable. Enhanced interaction of potassium was already noted by Aydin et al. for slightly wider tubes and is reminiscent of the long-known complexation of cations with benzene, "cation-$\pi$ interaction".[54] Partly but less significantly, the differences between the ions are also related to different arrangement of water molecules and water-water interaction around the ion, different for cations and anions. We also note that proton transfers about as favorably as $K^+$. Practically, that means that, in experiments that involve KCl solutions, $K^+$ will outcompete the more dilute protons and must be the dominant cation species within CNTPs.

However, uptake of $K^+$ is subject to limitations imposed by the requirements of overall electroneutrality. The latter will always apply whenever potential variations in CNTP are sufficiently smeared by either the screening length being shorter than CNTP length[55] or ion charge delocalization via bonding to CNTP.[47] Electroneutrality dictates that the uptake of a $K^+$ cation needs to be counter-balanced by uptake of an anion, either $Cl^-$ and $OH^-$, both having a highly unfavorable $\Delta G^{ex}$. As the simplest mean-field approximation, we may assume a uniform mean potential $\phi$ within the CNTP relative to bulk thus ion uptake is given by

$$\sum_{i\ (cations)} C_i \exp\left(-\frac{\Delta G_i^{ex} + F\phi}{RT}\right) = \sum_{j\ (anions)} C_j \exp\left(-\frac{\Delta G_j^{ex} - F\phi}{RT}\right), \tag{1}$$

where $C$'s are respective cation and anion concentrations in solution. The exponents are essentially ion partitioning coefficients, calculated by solving this equation for $\phi$, given $\Delta G^{ex}$ for all ions. $\Delta G^{ex}$ should be understood as the appropriate statistical means, reflecting ion-ion interactions as well. Yet, in the simplest picture, when ions are assumed to collectively preserve electroneutrality but, otherwise, do not significantly interact with each other, we approximate $\Delta G^{ex}$ by the values computed for individual free ions. We consider available experimental data on ion transport in CNTPs along with present *ab initio* results to judiciously select the ions that need to be considered in eq. 1. Most measurements yield ion permeabilities rather than partitioning, therefore the differences in ion mobilities need to be considered as well. However, as water in the 0.8 nm CNTP is still not too much more constrained compared with bulk water and neither are ions, their mobility should not drastically differ from the bulk values. Indeed, inspection of reported estimates of water diffusion within (6,6) tubes obtained by experiments and simulations show that virtually all of them vary within fairly narrow range between 0.89 and 4.4 × $10^{-9}$ $m^2/s$. This range contains even more narrow range from 1 to 2.5 × $10^{-9}$ $m^2/s$ covering all reported diffusivity values for water and potassium and lithium cations in 1 and 1.5 nm tubes, as well as bulk mobilities of these species and chloride (see Supplementary Information). Proton and hydroxide ions are well-known exceptions, as they employ the much faster Grotthuss mechanism. MD simulations by Lee et al., modified to allow water dissociation, placed diffusivities of both ions in (6,6) tubes in the similar range 19 to 32 × $10^{-8}$ $m^2/s$, with smaller values corresponding to shorter tubes.[56] Dellago et al. obtained a fairly close value 17 × $10^{-8}$ $m^2/s$ for proton using *ab initio* computations.[57] Notably, the uncertainties for water and regular ions stay within a factor 5 from each other and, for proton and hydroxide, within a factor of 2. On the transfer energy scale, this is equivalent to 4 and 2 kJ/mol, respectively, i.e., within the error of *ab initio* computations. Given such insignificant uncertainties of mobilities, we deem it most expedient to simply adopt for subsequent calculations the bulk values 2 × $10^{-9}$ $m^2/s$ for potassium and chloride mobilities and, for hydroxide, Lee et al's estimate for shortest (6,6) tubes, 24 × $10^{-8}$ $m^2/s$.

When KCl transfers as free ions subject to electroneutrality and the effect of pH is negligible, i.e., $H^+$ and $OH^-$ do not affect salt uptake, $K^+$ and $Cl^-$ hence salt concentrations within CNTP, denoted with a bar, will all be about identical and linearly depend on the salt concentration in solution $C_s$, as follows

$$\bar{C}_s = \bar{C}_K = \bar{C}_{Cl} = C_s \exp\left(-\frac{\Delta G_K^{ex} + \Delta G_{Cl}^{ex}}{2RT}\right), \tag{2}$$

The average $\Delta G_s^{ex} = \frac{1}{2}(\Delta G_K^{ex} + \Delta G_{Cl}^{ex})$ essentially plays here the role of excess Gibbs energy for pH-independent salt transfer. However, the non-linear scaling of conductivity observed at pH 7.5 in Fig. 2a indicates that such a pH-independent scenario operates only at low pH. Apparently, pH comes into play in neutral conditions as preferential uptake of $OH^-$ ions, as reported for wider tubes and observed in *ab initio* simulations of graphene surfaces in water.[27,58] When OH$^-$ is strongly favored over Cl$^-$, eq. 1 has to be replaced with

$$\bar{C}_K \approx \bar{C}_{OH} \approx (C_s C_{OH})^{1/2} \exp\left(-\frac{\Delta G_K^{ex} + \Delta G_{OH}^{ex}}{2RT}\right), \tag{3}$$

where $C_{OH} = 10^{pH-14}$ in M units. The unusual 1/2 scaling of conductivity with $C_s$ predicted by eq. 3 and observed by Tunuguntla et al at pH 7.5 is a signature of such a pH-dependent ion partitioning.[35] In this scenario, the potassium mainly transfers in combination with hydroxide, i.e., KOH, with a transfer energy $\Delta G_h^{ex} = \frac{1}{2}(\Delta G_K^{ex} + \Delta G_{OH}^{ex})$ replacing $\Delta G_s^{ex}$. On the other hand, Cl$^-$ will transfer as a trace species and its concentration in CNTP will be given by

$$\bar{C}_{Cl} \approx C_s^{3/2} C_{OH}^{-1/2} \exp\left(-\frac{2\Delta G_{Cl}^{ex} + \Delta G_K^{ex} - \Delta G_{OH}^{ex}}{2RT}\right) = C_s^{3/2} C_{OH}^{-1/2} \exp\left(-\frac{2\Delta G_s^{ex} - \Delta G_h^{ex}}{2RT}\right), \tag{4}$$

Since, as the minority species, Cl$^-$ controls KCl permeability in this regime, the salt and Cl$^-$ permeation rates should scale with salt concentration as $C_s^{3/2}$ and the quantity $\Delta \tilde{G}_s^{ex} = \Delta G_s^{ex} - \frac{1}{2}\Delta G_h^{ex}$ should replace $\Delta G_s^{ex}$ for chloride transfer in this scenario. Along with 1/2 scaling of conductivity, these features are another signature of the pH-controlled ion transfer. Obviously, when OH$^-$ concentration drops, e.g., by 4.5 orders of magnitude at pH 3, this regime should transition to ”regular” linear KCl transfer.

Li et al.[46] measured chloride permeation rates using stop-flow experiment in vesicles and derive chloride permeability in CNTPs $P_{Cl}$ by fitting the anion permeation rate to a linear dependence on $C_s$. However, the observed trend was clearly non-linear and a much better fit is obtained for $C_s^{3/2}$ scaling, in agreement with eq. 4, as shown in Fig. 2b (see also Supplementary Information Fig. S5). We also find that the computed $\Delta \tilde{G}_s^{ex} = 62.6$ kJ/mol (for $\epsilon = 2$) fully agrees with the value 63 kJ/mol obtained by viewing it as a parameter and fitting eq. 4 with mobilities estimated as explained above to measured permeation rates in Fig. 2b. We also note that $P_{Cl}$ of chloride derived from above stop-flow anion permeation experiments in vesicles for similar solution compositions at pH 7.5 is of the order $10^{-18}$ - $10^{-17}$ $\mathrm{cm}^3/\mathrm{s}$, equivalent to conductance $\frac{F^2}{RT}C_{Cl}P_{Cl}$ of a few fS per channel. On the other hand, electrical measurement by Tunuguntla et al. in Fig. 2a show a much larger electrical conductance of the order 2-30 pS per channel at this pH. In addition, these authors also estimated ion transport numbers using reverse potential measurements.[25] Potassium transport number $t_K$ was found to be under 0.1 at pH 7.5, as reasonable when the rest of the current is carried by highly mobile hydroxide. The small chloride permeability measured in stop-flow experiments at pH 7.5 is then another manifestation of chloride being a minority anionic species within CNTP at this pH. Yet, $t_K$ increased to about 0.65-0.85 at pH 3, as expected when chloride takes over as the dominant anion.

Here we note that the above results also rule out the alternative mechanism, often discussed on the context of ion selectivity in CNTPs, whereby weakly acidic groups at the rim are presumed to repel anions and thus control ion transfer. As the acidic charges are active at pH 7.5 and neutralized at pH 3, the anion permeation should be more suppressed at higher pH and their transport number should drop and that of cation increase. This clearly disagrees with observations, as Li et al. report that permeation rates of chloride and other halides do not change significantly between the two pH.[46] Along with conductivity measurements of Tunuguntla el al. showing a much larger cation transport number at lower pH,[25] this makes it unlikely that acidic groups at the rim contribute significantly to ion transfer resistance.

In another report, Tunuguntla et al. employed permeation in vesicles loaded with a pH sensitive dye at pH 7.5 to measure proton transfer rates in CNTPs under a pH gradient.[26] The observed rates were interpreted as a fast proton transfer, presumably involving the Grotthuss mechanism. We note, however, that proton flux $J_H$ is indistinguishable from oppositely directed transfer of hydroxide $J_{OH}$ or simultaneous transfer of both ions in the form of alkalinity flux $J_{OH}-J_H$. The present analysis strongly suggests the actual permeating species was $\mathrm{OH}^-$. The higher affinity of narrow CNTPs to hydroxide also readily explains their larger

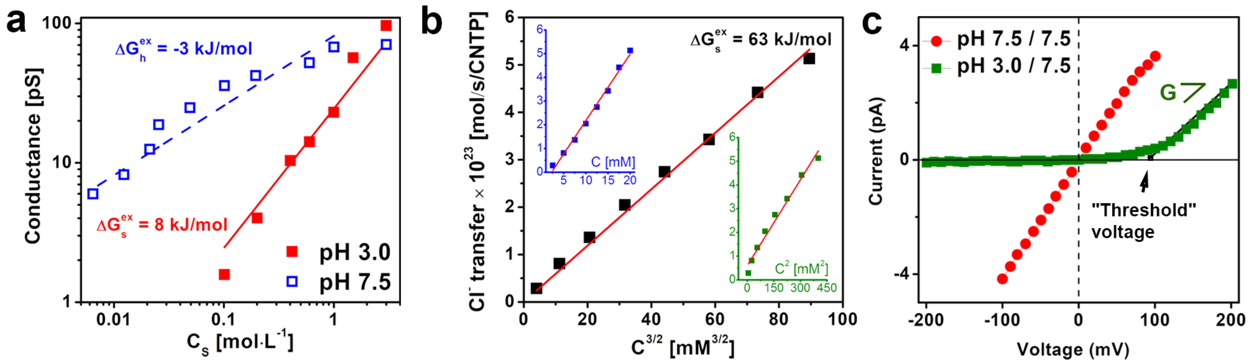

Figure 2: **Key experimental results on ion transport in 0.8 nm CNTPs**. (**a**) CNTP conductivity in KCl solutions at pH 3 and 7.5 reported by Thunuguntla el al.[25] Solid and dashed lines were computed using, respectively, eqs. 2 and 3 with mobilities estimated based on Dellago et al.[57] and $\Delta G_s^{ex}$ and $\Delta G_h^{ex}$ viewed as adjustable parameter with best-fit value indicated. (**b**) Rate of chloride permeation per CNTP measured in vesicles at pH 7.5 vs. $C_s^{3/2}$, as reported by Li et al.[13] Solid line is a linear fit to eq. 4 with mobilities estimated based on Dellago et al.[57] and $\Delta \tilde{G}_s^{ex}$ viewed as fitting parameters with best-fit value indicated. The insets highlight non-linear dependence obtained by plotting the same data vs. $C_s$ and $C_s^2$. (**c**) Current-voltage dependence of CNTP connecting two 0.1 M KCl solutions of pH 3 and 7.5 (green squares) and of the same pH 7.5 (red circles), reported by Tunuguntla et al.[25] All data were digitized from original reports.

conductivity, compared with wider 1.5 nm CNTPs. The measured rate of alkalinity transfer is equivalent to a conductance of the order 1 fS, again, commensurate with anion transfer data, yet four orders of magnitude smaller than results of conductivity measurements. This discrepancy manifests coupling of alkalinity transfer, i.e., $OH^-$ permeation, to much slower transfer of $K^+$. In absence of electric current, its rate is limited by $K^+$ diffusivity and may no more benefit from the fast Grotthuss mechanism. The reported blocking effect of $Ca^{2+}$ is also consistent with this picture, as it should bind to CNTP more strongly and have a lower mobility than $K^+$ due to double charge and thus further slow down hydroxide permeation.

Finally, activation energies $E_a$ of permeation offer yet another way of comparing present model with experiments. They should be dominated by the enthalpies of ion transfer, i.e., $\Delta H$, displayed in Fig. 1h as well. For instance, Li et al.[13] reported activation energies for permeation of halide anions, however, the present model indicates they may not be compared directly with $\Delta H$ for respective anions due to coupling to other ions. Thus, depending on whether eqs. 2 or 4 describes chloride transfer, the apparent activation energy for $\mathrm{Cl}^-$ permeation should be - using notation analogous to $\Delta G^{ex}$ - either $\Delta H_s$ or $\Delta\tilde{H}_s$, respectively. Li et al.'s reported $E_a = 52$ kJ/mol for chloride permeation in vesicles, which they compared with computed chloride transfer energy 63 kJ/mol. It is unclear why the latter value, computed for CNTP in vacuum ($\epsilon = 1$), is so different from the present $\Delta H_{Cl} \approx 166$ kJ/mol for $\epsilon = 1$ and is much closer to the present result for $\epsilon = 100$. We presume this might be affected by the fact that, in computations by Li et al., CNTP was connected to highly polarizable graphene sheets, which could strongly reduce the dielectric contribution by essentially "grounding" the CNTP. Nevertheless, the activation energy of chloride transfer may not be identified with $\Delta H_{Cl}$ in either case and the agreement could be fortuitous.

The present analysis suggests that observed $E_a = 52$ kJ/mol of chloride permeation should be compared with either $\Delta H_s \approx \frac{1}{2}(-37.1 + 121.7) = 42.3$ kJ/mol for the pH-independent scenario, eq. 2, or with $\Delta\tilde{H}_s = \Delta H_{Cl} + \frac{1}{2}(\Delta H_K - \Delta H_{OH}) \approx 121.7 + 0.5 \times (-37.1 - 122.4) = 42.0$ kJ/mol for pH-controlled one, eq. 4. These values are close, due similar transfer energies for chloride and hydroxide and may not differentiate between the two theoretical expressions, however, the scaling of conductivity and permeation rate with $C_s$ in Fig. 3 strongly favors $\Delta\tilde{H}_s$ as the appropriate one. The difference between observed $E_a$ and appropriate $\Delta H$ may come from unaccounted for activation energy of diffusion, which may be fairly close to that of water discussed above, 15-20 kJ/mol, and add to $E_a$ accordingly. On the other hand, sensitivity to $\epsilon$ (see Fig. 2) presents another substantial uncertainty. For instance, replacing $\epsilon = 2$ with $\epsilon = 2.4$, better representing lipids,[53] reduces $\Delta H$ by about 20 kJ/mol.

In a similar manner, eq. 4 predicts that the activation energy for alkalinity permeation should be $\Delta H_h = \frac{1}{2}(\Delta H_K + \Delta H_{OH}) \approx 0.5 \times (-37.1 + 122.4) = 42.6$ kJ/mol for $\epsilon = 2$. This is fairly close to the experimental value 55 kJ/mol reported by Tunuguntla et al.[25] The difference could again come from unaccounted for activation energy of diffusion and the sensitivity of transfer energies to $\epsilon$. Another factor is deviations from the simple mean-field picture, i.e., ion-ion interactions that should reduce the transfer energies, as analyzed next.

## The puzzle of hydroxide: why it is favored and how it conducts

Above comparison with experiments demonstrate that computed values of $\Delta G^{ex}$ for free ions combined with simple mean-field relations may rationalize most experimental observations and trends. However, two points raise questions. First, despite the fact that the $C_s$ scaling of experimental data in Fig. 2 strongly suggests that CNTP has a strong preference to hydroxide, transfer energies of single chloride and hydroxide anions in Fig. 1h do not display as much difference. In addition, viewing $\Delta G_s^{ex}$ and $\Delta G_h^{ex}$ as adjustable parameters and fitting them to the conductivity data at pH 3 and 7.5 to eqs. 2 and 4, respectively, yields $\Delta G_s^{ex} \approx 8$ kJ/mol and $\Delta G_h^{ex} \approx$ -3 kJ/mol that are significantly different from the present *ab initio* estimates (see Fig. 2a and Supplementary Information for detail). We may only speculate below as to why these fits deviate so much from theoretical values that, otherwise, reasonably agree with stop-flow permeation data. However, the much different fitted $\Delta G_s^{ex}$ and $\Delta G_h^{ex}$ once again manifest a high affinity of CNTP to hydroxide and it is necessary to consider more involved scenarios that would favor this ion.

Second, concurrent permeation of free cations and anions, like in stop-flow experiments in vesicles, may proceed with minimal mutual interference, however, in electrical measurements, ions migrate in opposite directions and, at some point, meet and need to pass each other. It is not obvious whether squeezing ions past each other in a narrow channel does not present a prohibitive kinetic barrier. Admittedly, this barrier would be eliminated in a scenario recently analyzed by Levy et al. who argued that electroneutrality could break down in a narrow and short channel thereby ions could pass the entire channel one at a time.[55] This mechanism was justified on the ground that screening length in a CNTP becomes exponentially large due to 1D dimensionality of the "solution" in a narrow channel. However, in such a scenario, $K^+$ transfer as a lone charge carrier would be decoupled from $OH^-$ and, instead, coupled to $Cl^-$. Indeed, we do not anticipate any ion-specific effect in solution outside CNTP therefore far more dilute hydroxide would be unable to outcompete chloride and would have a negligible effect on potassium transfer. Conversely, hydroxide transfer as a lone species within CNTP must be strongly suppressed by its prohibitive transfer energies (Fig. 1h), which disagrees with its high transfer number. It seems that experimental data and present *ab initio* results rule out the electroneutrality breakdown mechanism.

A more plausible alternative is that the system may substantially deviate from the simple mean-field picture due to ion-ion interactions. Specifically, when ions approach each other, the electrostatic part of the highly unfavorable interaction of anions with CNTP may be attenuated or, when ions associate, eliminated thus ion-specific effects may come into play. As a proxy of such situation, we consider ion pairing, thereby ions within CNTP may be present as coexisting pairs and free ions. Essentially, this model is a one-dimensional analogue of the Bjerrum model of electrolytes solutions, in which ions pairs coexist with a free-ion solution treated in the mean-field manner.[59] Although the need to squeeze cation and anion past each other to allow conduction may not be avoided, $OH^-$ uptake within a pair could become more favorable and reduce the corresponding barrier as well. Analyzing this scenario requires transfer energies for pairs formed within CNTP, which we compute here *ab initio.*

Figure 3a shows transfer energies of the possible contact ion pairs (CIP) in (6,6) CNTP in vacuum and $\epsilon = 2$, along with trasfer energy of the same combination as free non-interacting ions (F), i.e., average of the two single-ion transfer energies, shown as empty bars.To reduce computational costs, we consider simply the electronic transfer energy $\Delta E$, given $\Delta E$ and $\Delta G^{ex}$ show identical trends and reasonably small differences for free ions (see Supplementary Information). It is immediately notable that the KOH pair has an exceptionally low transfer energy compared to the other pairs, which may now rationalize the strong preference of narrow CNTPs for $OH^-$ over $Cl^-$. Similar to water, which is formally the $H^+OH^-$ pair, the transfer energies of all ion pairs $\Delta E_{pair}$ are weakly affected by $\epsilon$. Compared to transfer energy of the pair as free ions, i.e., $\frac{1}{2}(\Delta E_+ + \Delta E_-)$, there is a gain of several tens kJ/mol for all salts. However, $\Delta E$ or $\Delta G^{ex}$ for pairs and free ions may not be directly compared, since pairing also involves a significant entropy loss. Considering dilute solutions and neglecting the solution non-ideality and different sizes of ions and pair, the concentration of KOH pairs in CNTP is given by

$$\bar{C}_{KOH} = \frac{C_K C_{OH}}{C_w} \exp\left(-\frac{\Delta G^{ex}_{KOH}}{RT}\right), \tag{5}$$

where $C_w = 55.6$ M in the denominator comes from the fact that the ideal solution entropy needs to be computed using concentrations expressed in molar fractions. We compare eqs. 2 and 5 and, specifically, consider the exponential factor that multiplies in eq. 2 the product $(C_K C_{OH})^{1/2}$ that gauges the activity of the KOH "salt" in solution. This shows that the free-ion transfer energy $\Delta G^{ex}_{h} \approx 62.6$ kJ/mol (for $\epsilon = 2$) in eq. 2 is to be compared with $\Delta G^{ex}_{h,pair} = \Delta G^{ex}_{KOH} + RT \ln[C_w/(C_K C_{OH})^{1/2}]$ for KOH uptake as ion pairs. The second term in the last expression accounts for the loss of translational entropy upon pairing and, for $C_s$ in the range $10^{-3}$ to 1 M and $3 \leq pH \leq 7$, it amounts to about 30 to 50 kJ/mol. To complete this analysis, we obtained using Gaussian's thermochemical package $\Delta G^{ex}_{KOH}$ = -61.6 kJ/mol for $\epsilon = 2$, which turns out to be only slightly above $\Delta E_{KOH}$ (see Fig. 3). Ultimately, the terms sum up to $\Delta G^{ex}_{h,pair} \approx$ -31 to -11 kJ/mol for the above composition range. It is obviously far below the free-ion counterpart and indicates that majority of $K^+$ and $OH^-$ ions partition to CNTP as KOH pairs.

Similar analysis for the other pairs shows that, even if their formation is not as favorable as KOH, they are likely to contribute at least as much as corresponding combination of free ions (CIP vs F bars in Fig. 3a). While pairs represent only the simplest form of ion-ion interactions deviating from mean-field treatment, present analysis highlights the crucial role of such interactions in controlling ion partitioning and transport in CNTPs and, in particular, high affinity towards $OH^-$. We note, however, that presence of pairs in CNTP does not necessarily directly translate to transport, since pair mobility may be small. Indeed, we note that, in the case of chloride permeation, if this ion was mainly transferred as KCl pairs, its permeation rate would be proportional to $C_s$ squared. The inset in Fig. 2b (see also Fig. S5 in Supplementary Information) indicate this scaling disagrees with experiment and ruling it out questions any significant contribution of ion pairs to ion permeation by diffusion.

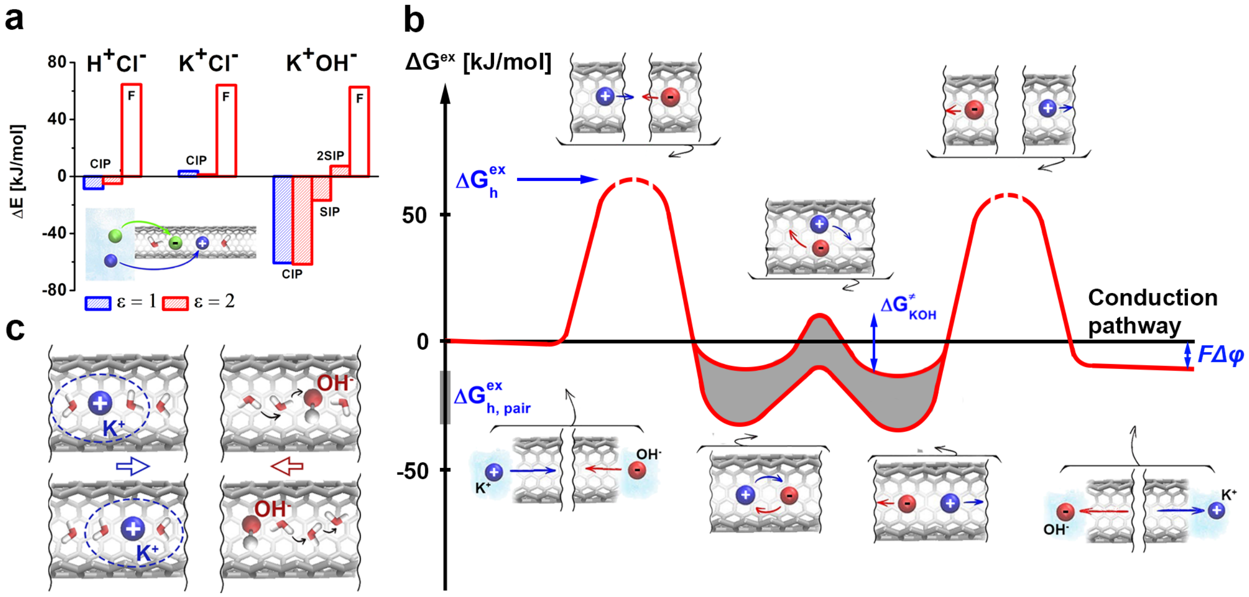

Figure 3: **Ion pair formation and conduction mechanism in (6,6) CNTP.** (**a**) $\Delta G^{ex}$ of ion-pair formation in CNTP for different ion pairs for $\epsilon = 1$ and $\epsilon = 2$; F denotes free ions, CIP contact pairs, SIP - pair separated by one water molecule, 2SIP - pair separated by two water molecules. (**b**) Schematic energy profile encountered by the potassium and hydroxide ions along the conduction pathway, including free-ion uptake, downfield migration, transient pair formation, flip, and dissociation. (**c**) Possible mechanism of electro-osmosis: water flow coupled to potassium migrations and decoupled from hydroxide migrating by the Grotthuss mechanism.

## CNTP conductance: what is the rate-controlling step

Even if abundant within CNTP, pairs may not contribute to conductance not only due to low mobility, but also since they are neutral and cannot carry an electric current. A cation and an anion migrating in an electric field in the opposite directions may then temporarily form a pair, however, it will have to flip and split up thereafter to let the ions keep migrating. In the spirit of the Eyring-Polanyi transition-state theory, we may consider the flip and its Gibbs energy $\Delta G^{\neq}_{KOH}$ relative to the ”ground state” of the pair aligned parallel to the main CNTP axis. Presumably, the height of the kinetic barrier correspond to the pair aligned perpendicular to the CNTP main axis. We estimated this height to be $\Delta G^{\neq}_{KOH} \approx 23$ kJ/mol above the ”ground state” $\Delta G^{ex}_{h,pair}$, which places the barrier height at -8 to 12 kJ/mol relative to the solution. It is well below the free-ion energy $\Delta G^{ex}_{h} \approx 62.6$ kJ/mol ($\epsilon = 2$). We then conclude that CNTP conductance should indeed be controlled by the partitioning and transport of free ions, in agreement with most experimental data. Figure 3b schematically depicts the suggested pathway and energy profile encountered jointly by the potassium and hydroxide ions upon conduction. It starts from their uptake as free ions from solution at opposite ends of CNTP, followed by free-ion migration, pair formation, flip, dissociation back to free ions, and, ultimately, exit to the solution at the opposite end. The entire profile is slightly inclined due to electric potential difference applied along the nanotube $\Delta\varphi$ and the shown sequence may repeat, if CNTP contains more than one pair. The larger number of KOH pairs relative to other possible pairs, due to exceptionally low $\Delta G^{ex}_{KOH}$, is apparently the reason behind the hydroxide dominating ion conductance at neutral conditions.

One may ask what happens to water molecules within CNTP when $K^+$ and $OH^-$ (or $Cl^-$) migrate in electric field and induce an electro-osmotic flow of water, as demonstrated for wider 1.5 nm CNTPs.[40] The partitioning-controlled scaling of conductivity with $C_s$ suggests electro-osmosis in single-digit CNTPs is apparently not as strong as in wider tubes. Yet, if both ions experience strong friction with water, ions will hinder each other's migration. Indeed, when the ion with the larger friction dictates the ultimate direction of electro-osmosis, the other will be forced to squeeze past all water molecules, in a manner similar to the ion pair flip. However, the Grotthuss mechanism may help circumvent this obstacle, permitting a nearly friction-less $OH^-$ transfer as a fast shuttling of electron and hydrogen between $OH^-$ and a neighboring water molecule followed by minor local atom rearrangement. This may readily occur against water flow and will not interfere with the electro-osmosis induced by $K^+$ migration, minimizing this ion's friction with water as well. This mechanism, whereby $OH^-$ ions may rapidly migrate downfield regardless of electro-osmosis induced by potassium, is schematically illustrated in Fig. 3c and may explain insignificant electro-osmosis in (6,6) tubes and the large transport number of $OH^-$ at pH 7.5. Note that, within this picture, the ion pair flip is still required, otherwise $K^+$ will separate between the $OH^-$ ion and next water molecule and prevent shuttling of electron and hydrogen.

At this point, we note that, in reality, there is obviously no sharp distinction between free ions and pairs assumed in our highly simplified picture. The long-range nature of the electrostatic attraction between cation and anion must smear the heights and valleys of the profile in Figure 3b. Perhaps more importantly, the ion-ion interaction should both eliminate a part of the dielectric energy and allow anions interact more favorably with CNTP walls. This should reduce the free-ion transfer energy well below simple combination of single-ion transfer energies. To illustrate this point, we also computed and display in Fig. 3a the transfer energies of the KOH pairs separated by one (SIP) and two water molecules. The transfer energy clearly increases with ion-ion separation, but it may still remains noticeable below the free-ion value over distances of a few nanometers, reducing the average transfer energy. This might partly explain why very low $\Delta G_s^{ex}$ and $\Delta G_h^{ex}$ fitted to conductance data and shown in Fig. 2a are closer to $\Delta G^{ex}$ for corresponding pairs with pairing entropy correction than to their free-ion counterparts. On the other hand, the rates and activation energies of chloride and alkalinity permeation measured in stop-flow experiments agree better with the simple free-ion estimates. Not unlikely, part of the answer may have to deal with the fact that the conductivity is controlled by the faster ion of the pair, i.e., $OH^-$ in the case of KOH, while the permeability measured in stop-flow experiments is determined by the slower one, i.e., $K^+$. We also speculate that effects absent or ignored in the present analysis, e.g., alternative conduction paths, or different settings and CNTP environment in electrical and stop-flow measurements, changing the effective value of $\epsilon$, may affect the results. We presume these questions will be clarified, as more data on ion transport in CNTPs become available.

## Current rectification explained

Finally, we will show that the strong dependence of conductance on $OH^-$ readily explains current rectification between solutions of different pH and, specifically, blockage of current in the direction from low to high pH. The mean-field relation, eq. 3, may be incorporated in

Nernst-Planck-type relations, which yields the following relation between the current ($I$) and applied voltage ($\Delta\varphi$) and solution composition differences (see Supplementary Information for derivation)

$$I = G\left(-\Delta\varphi + t_{OH}\frac{RT}{F}\Delta\ln C_{OH} - t_K\frac{RT}{F}\Delta\ln C_K\right), \tag{6}$$

where $\Delta$ designates differences between the two solutions and $t_{OH}$ and $t_K$ are respective ion transport numbers within CNTP. $G$ is the effective CNTP conductivity, having the following dependence on the solution concentrations

$$G \propto \frac{\Delta(C_K C_{OH})^{1/2}}{\Delta\ln(C_K C_{OH})^{1/2}} = \langle (C_K C_{OH})^{1/2}\rangle_{l.m.}, \tag{7}$$

where the omitted proportionality constant accounts for the partitioning (related to the transfer energies), ion mobilities and CNTP geometry. Eq. 7 shows that $G$ is proportional to the logarithmic mean of the products $(C_K C_{OH})^{1/2}$ of the two solutions, thereby it is mainly determined by the solution with the larger $(C_K C_{OH})^{1/2}$. For instance, in experiments by Tunuguntla et al.,[25] displayed in Fig. 2c, current rectification was observed between solutions with pH 7.5 and 3 containing 0.1 M KCl on both sides (green squares). The driving force, i.e., expression in brackets in eq. 6, depends on both pH values and becomes zero when the applied potential equals the threshold voltage indicated in Fig. 2c. Above this potential, the conductance $G$, i.e., the I-V slope, determined by pH 7.5, is indeed similar to the case when both solutions have the same pH 7.5 (red circles in Fig. 2C). However, the conductance sharply drops and current is blocked below this potential due local pH changes induced by polarization.

Equations 6 and 7 predict no rectification, yet it may come from concentration polarization, i.e., ion depletion or enrichment in solution next to CNTP mouth, when a DC current enters or exits CNTP. The above rectification experiments were performed in presence of large concentrations of salt. The transport of salt ions, in particular, potassium is then not a limiting factor and the key limitation comes from the depletion of $OH^-$ ions in solution

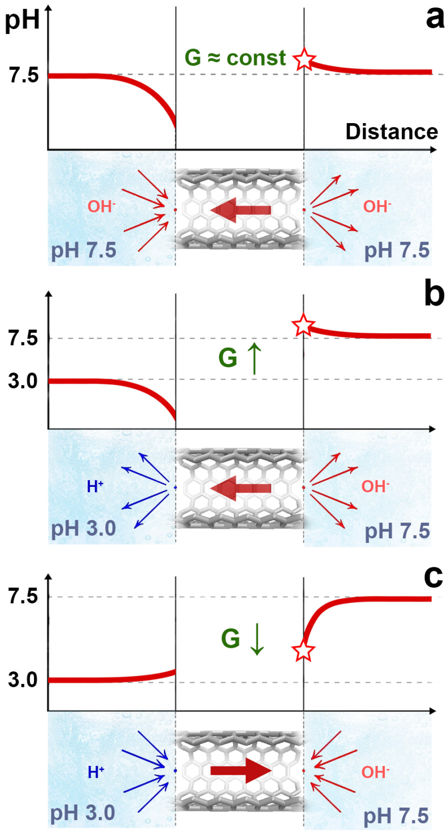

Figure 4: **The mechanism of current rectification in CNTP between two solutions.** (**a**) Solutions of the same pH: applied voltage and passing of current weakly affects CNTP conductance, showing no rectification. (**b**) Voltage applied in forward direction from high to low pH: local pH raised at high pH end results a minor increase in CNTP conductance, no current blockage. (**c**) Voltage applied in backward direction from low to high pH: local pH drops at high pH end results in a major drop in CNTP conductance, blocking the current. Large red arrows indicates current direction. Thin arrows next to CNTP mouths indicate ion diffusion, resulting in concentration polarization and a change in local pH. The star indicates local pH controlling CNTP conductivity.

next to a CNTP mouth. The large salt concentration also facilitates the analysis, since it eliminates the potential gradients in the solution. Thus the depletion or enrichment of $OH^-$ is controlled primarily by its diffusion away from or towards CNTP and the magnitude and direction of the flow of $OH^-$ ions, i.e., the fraction of the current carried by $OH^-$, $It_{OH}$. Different situations encountered in conduction and rectification experiments are schematically illustrated in Fig. 4. To obtain the limiting value of $It_{OH}$ and total current, consider semi-spherical boundary layer of solution centered at CNTP mouth. The $OH^-$ concentration at the mouth will depend on $It_{OH}$ and the bulk concentration as follows[14]

$$C_{OH,mouth} = C_{OH,bulk} \pm \frac{It_{OH}}{2\pi F D_{OH} r_c}, \tag{8}$$

where $D_{OH}$ is the $OH^-$ diffusivity in solution, $r_c$ is the channel radius, and the sign is positive or negative when $OH^-$ ions move away from or towards the CNTP. According to eq. 7 conductivity will be controlled by the higher pH faced by CNTP, marked with the star Fig. 4. Thus the higher pH will always rise and the current will flow unobstructed, when CNTP faces two identical solutions (Fig. 4a). Similarly, no blockage will be observed when the current - by definition, opposite to $OH^-$ flow - is towards the low-pH solution, since it increases $C_{OH,mouth}$ at high-pH end and hence $G$, as shown in Fig. 4b. However, as depicted in Fig. 4C, when the current reverses, $C_{OH,mouth}$ at high-pH end drops, sharply reducing $G$ and blocking the current. Since chloride does not allow as much conductivity as hydroxide (cf. Fig 2a), we ignore the takeover by chloride at low pH and take the maximal (limiting) current $I_{lim}$ as approximately corresponding to $C_{OH,mouth} = 0$. Using $D_{OH} = 6.8 \times 10^{-9}$ $m^2/s$, $r_c = 0.4$ nm, $t_{OH} = 0.9$, and $C_{OH,bulk} = 10^{-6.5}$ M (pH 7.5), we estimate $I_{lim} = (2\pi F D_{OH} r_c C_{OH,bulk})/t_{OH} \sim 1$ fA, which is is far smaller than pA currents measured in forward direction, thereby backward current will be effectively blocked, i.e., rectification will be observed. More accurate relations, accounting for the pH changes at both ends and yielding the entire I-V curve may be easily developed, by combining eqs. 6 and 7 with mass transfer in solutions,[14] but they do not change the above conclusion. Note, the full model must also address the fact that $It_{OH}$ flows in solution as an alkalinity flow, carried by both $OH^-$ and $H^+$ . The effective diffusivity of $OH^-$, yielding the total alkalinity flux, then becomes pH-dependent, $D_{OH} + D_H 10^{14-2pH}$. Obviously, the actual species carrying most alkalinity flow in pH 3 solution (and, in general, at any pH $\leq 7$) is $H^+$ rather than $OH^-$, as indicated in Fig. 4b and c.

At this point, we note that the very small limiting current (i.e., large access resistance) of $OH^-$, responsible for current rectification, is due its very low concentration in solution at pH 7.5. Salt ions, $K^+$ and $Cl^-$, have much higher concentrations and are unlikely to produce such effect. Relevant salt concentrations substituted to eq. 8 yield limiting transfer rates equivalent to currents of the order tens to thousands picoamperes or molar flow rates $10^{-17}$ to $10^{-15}$ mol/s per CNTP (see Supplementary Information). As these are far larger that the measured currents and permeation rates in Fig. 2, the access resistance for this ions should have no affect on the measured transport characteristics of CNTP.

## Conclusions

We have demonstrated that most experimental data on ion transport in narrow (6,6) CNTPs, including both diffusion or electrical measurements, may be rationalized using presented molecular model, as alternative to commonly considered continuum-like models. The model treats ion partitioning in the mean-field manner considering uptake of free ions, subject to electroneutrality, to which ion pairing is added to better account for ion-specific effects, with all relevant thermodynamic quantities computed *ab initio*. We note that, despite the fact that experimental data and their pH and salt concentration dependence strongly suggest a high affinity of (6,6) CNTPs towards hydroxide, the computed transfer energies for single ions do not indicate any such preference. However, computations for ion pairs do reveal a strong affinity to hydroxide, as the exceptionally favorable transfer energy for the KOH pair. In experiments with KCl solutions, this makes $K^+$ and $OH^-$ ions dominant species within CNTP at neutral conditions, which change to $K^+$ and $Cl^-$ in acidic conditions. We conclude that the ion transport is apparently controlled by free ions, coexisting with more abundant, but less mobile ions pairs. This also makes hydroxide ions the main charge carrier species in conductance experiments, contrary to the views in the literature considering potassium as the main charge carrier. The model successfully explains most observed effects of salt concentration and pH on conductivity and anion and alkalinity permeation in stop-flow experiments, current rectification, and measured activation energies, as well as molecular mechanisms behind ion transfer and conductance in narrow CNTPs. The only significant discrepancy is found for ion transfer energies fitted to conductivity data, which yields values lower and, as a result, ion permeability higher than model predictions. Presumably, this may be related to the ion-ion interactions that may reduce transfer energy for anions and may be clarified, as more data become available. The proposed modeling approach may be extended to other sub-nanometer nanochannels and help design next-generation desalination and osmotic energy harvesting materials and devices.

# Methods

## Computational Details

The transfer of $H_2O$ and ions ($H^+$, $OH^-$, $K^+$, and $Cl^-$) was computed for the metallic (5,5) and (6,6) nanotubes of diameters 0.68 and 0.80 nm, respectively. For both types, the CNTP fragments used in computations were 1.72 nm long. Thus (6,6) tube had seven elementary cells, each containing 24 carbon atoms and total 168 carbon atoms, with dangling bonds at the rims was terminated with hydrogen atoms. The species of interest (an ion or a water molecule) was placed in the center of CNTP and surrounded by four water molecules, two on each side, for (5,5) tube and by six water molecules, three on each side, for (6,6) tube. This was presumed to be sufficient for cancelling out distant water-water interactions, given ions mainly affect water structure up to the second hydration shell and only marginally the third one.[60,61] The CNTP with its content was embedded in a dielectric continuum of a dielectric constant $\epsilon$, viewed as a parameter. For evaluating the thermodynamics of hydration in bulk water, the species of interest was surrounded by 6 water molecules, forming a finite cluster embedded in a polarizable continuum of dielectric constant 78.36. Our earlier estimates showed that the use of larger clusters leads to only a marginal improvement, for instance, the difference in ion hydration between 6- and 7-molecule clusters was less than 2 kJ/mol.[47]

Published data were used to set up the initial cluster geometries for hydrated $H_2O$,[62–64] $H^+$,[65] $OH^-$,[65,66] $K^+$[67] and $Cl^-$.[68,69] To benchmark the computations for interactions of water and ion with aromatic CNT walls, the energies of $H_2O$ and $K^+$ binding to benzene were computed and compared with experimental values.

The geometries of all structures and thermodynamic properties were calculated *ab initio* in Gaussian 09 Rev. B.01.[70] The computations employed the combination of wB97X-D functional[71] including Grimme's D2 dispersion correction[72] and 6-31G(d,p) basis set, which was found to yield the best agreement with experimental data on hydration in water. The optimization of structures within CNTP was performed starting from several initial geometries; thereafter, the optimized structure with minimal total electronic energy ($E$) was selected for further analysis. The IEFPCM polarizable continuum model[73] was used to simulate dielectric continua. Zero-point correction energy was computed to convert electronic energies $E$ to enthalpies ($H$). This correction did not include the vibrational frequency scaling factor, as associated error at the chosen level of theory was under 1 kJ/mol and less than typical errors of *ad initio* computations.[74] Basis set superposition error (BSSE) was estimated using the Boys and Bernardi method[75] in water/ion clusters and in CNTPs. Apart from electronic energy, the required thermodynamic quantities, i.e., $H$, excess Gibbs energies ($G^{ex}$), and excess entropies ($S^{ex}$), included only the vibrational contributions computed by Gaussian, while rotational and translation contributions were discarded, as they consider corresponding motions of the cluster as a whole and are irrelevant for deriving thermodynamics variables for individual molecules or ions. The transition state of the ion pair flip was localized using the Berny algorithm. The transition state was identified as that with one imaginary vibration frequency. The pair flip barrier was calculated as the difference between the transition and ground (pair aligned with main CNTP axis) states. Ultimately, the thermodynamic quantities for the transfer of a species from bulk water to water-filled CNTP, $\Delta X[\text{Ion}]$, were computed using the following relation[47]

$$\Delta X[\mathrm{Ion}] = X[\mathrm{CNTP(H_2O)}_m\mathrm{Ion}] + X[(\mathrm{H_2O})_n] - X[\mathrm{CNTP(H_2O)}_m] - X[\mathrm{Ion(H_2O)}_n]. \quad (9)$$

The analogous expression for transfer of a cation $C^+$ and an anion $A^-$ from bulk solution and formation of an ion pair $C^+A^-$ within CNTP was as follows

$$\begin{aligned}\Delta X[\mathrm{C^+A^-}] = X[\mathrm{CNTP(H_2O)}_m\mathrm{C^+}] + 2X[(\mathrm{H_2O})_6] - X[\mathrm{CNTP(H_2O)}_m] - \\ - X[(\mathrm{H_2O})_6\mathrm{C^+}] - X[(\mathrm{H_2O})_6\mathrm{A^-}].\end{aligned} \quad (10)$$

Figure S1 in Supplementary Information schematically illustrates transfers processes defined by eqs. 9 and 10. Note that different hydration of cations ($K^+$, $H^+$) and anions ($Cl^-$, $OH^-$) resulted in different arrangement of three adjacent water molecules, resembling zigzag and triple-bonded structures of water in Fig. 1a and b, respectively. In turn, this could affect the terminal ("surface") energy of the corresponding ion-water and ion pair-water clusters within CNTPs. To ensure this energy is cancelled in above equations, the energy $X[\mathrm{CNTP(H_2O)}_m]$ corresponded to the arrangement resembling the one adjacent to the ion involved or the average of the two arrangements for the ion pairs.

## Benchmarking *ab initio* computations

The transfer quantities critically depend on the reference values for hydration in water. We then first benchmarked computational procedures versus experimental bulk hydration quantities. Fig. S2 in Supplementary Information demonstrate a good agreement between computed and experimental values. The deviations for hydration enthalpies $H$ are 3 to 7 % of the absolute values. Similar errors were obtained for excess Gibbs energies $\Delta G^{ex}$, but for much smaller entropic terms $T\Delta S^{ex} = \Delta H - \Delta G^{ex}$, the deviations were larger, 1 % for water molecule and $K^+$, 10 % for $Cl^-$, and ca. 30 % for $H^+$ and $OH^-$. These errors were considered acceptable, as they may also similarly bias the energies in the bulk and within

CNTPs and thus partly cancel out in transfer energies. Besides, the magnitude and sign of deviations, positive for cations and negative for anions, are highly unlikely to affect the physical picture developed here. The present values also agree within a few kJ/mol with computations using a higher level of theory[62,65,67] and computations using the conductor-like screening model.[76,77]

As another benchmarking, most pertinent to interactions with the inner walls of CNT, we computed the enthalpies of interactions of $H_2O$ and $K^+$ with benzene, for which both experimental data[78–80] and computations[80–84] were reported. Comparison with most accurate data,[79,80] presented in Fig. S2 in Supplementary Information, shows deviations under 4 kJ/mol of the computed enthalpy for $H_2O$ and 1 kJ/mol for $K^+$, within typical errors of *ab initio* computations. Our calculations also indicate a negligible interaction of benzene with $Cl^-$ with enthalpy close to zero, in agreement with other reports.[85,86] The agreement was significantly poorer when no dispersion correction was used. This and above results indicate that the selected level of theory (wB97X-D/6-31G(d,p)) with dispersion correction was adequate for the present study, given the problem of accurately predicting hydration and solvation energies *ab initio* still have many issues.[87]

## Acknowledgements

The financial support by a joint grant 2016627 from the United States-Israel Binational Science Foundation (Israel) and National Science Foundation (USA) is acknowledged. The authors thank Aleksandr Noy and Meni Wanunu for discussions and many valuable suggestions.

# Supporting Information Available

Supplementary information contains the additional details of quantum-chemical calculations, benchmarking of hydration energies and interaction with benzene, derivation of the relation for CNTP conductance, calculation of limiting rate of salt permeation, transfer parameters for ions and ion pairs obtained from *ab initio* calculations, compiled literature data of ionic mobilities in CNTPs, fitting of transfer excess Gibbs energies to experimental data on conductivity and anion permeation in vesicles, and interpolation of the water transfer energies.

# References

(1) Mark, A. Science and technology for water purification in the coming decades. *Nature* **2008**, *452*, 20.

(2) Werber, J. R.; Deshmukh, A.; Elimelech, M. The critical need for increased selectivity, not increased water permeability, for desalination membranes. *Environ. Sci. Technol. Lett.* **2016**, *3*, 112–120.

(3) Agre, P.; King, L. S.; Yasui, M.; Guggino, W. B.; Ottersen, O. P.; Fujiyoshi, Y.; Engel, A.; Nielsen, S. Aquaporin water channels–from atomic structure to clinical medicine. *J. Physiol.* **2002**, *542*, 3–16.

(4) Kidambi, P. R.; Jang, D.; Idrobo, J.-C.; Boutilier, M. S.; Wang, L.; Kong, J.; Karnik, R. Nanoporous atomically thin graphene membranes for desalting and dialysis applications. *J. Adv. Mater.* **2017**, *29*, 1700277.

(5) Jang, D.; Idrobo, J.-C.; Laoui, T.; Karnik, R. Water and solute transport governed by tunable pore size distributions in nanoporous graphene membranes. *ACS Nano* **2017**, *11*, 10042–10052.

(6) Wang, L.; Williams, C. M.; Boutilier, S. H., Michael; Kidambi, P. R.; Karnik, R. Single-layer graphene membranes withstand ultrahigh applied pressure. *Nano Lett.* **2017**, *17*, 3081–3088.

(7) Kidambi, P. R.; Terry, R. A.; Wang, L.; Boutilier, M. S.; Jang, D.; Kong, J.; Karnik, R. Assessment and control of the impermeability of graphene for atomically thin membranes and barriers. *Nanoscale* **2017**, *9*, 8496–8507.

(8) Hinds, B. J.; Chopra, N.; Rantell, T.; Andrews, R.; Gavalas, V.; Bachas, L. G. Aligned multiwalled carbon nanotube membranes. *Science* **2004**, *303*, 62–65.

(9) Holt, J. K.; Park, H. G.; Wang, Y.; Stadermann, M.; Artyukhin, A. B.; Grigoropoulos, C. P.; Noy, A.; Bakajin, O. Fast mass transport through sub-2-nanometer carbon nanotubes. *Science* **2006**, *312*, 1034–1037.

(10) Holt, J. K.; Noy, A.; Huser, T.; Eaglesham, D.; Bakajin, O. Fabrication of a carbon nanotube-embedded silicon nitride membrane for studies of nanometer-scale mass transport. *Nano Lett.* **2004**, *4*, 2245–2250.

(11) Werber, J. R.; Osuji, C. O.; Elimelech, M. Materials for next-generation desalination and water purification membranes. *Nat. Rev. Mater.* **2016**, *1*, 1–15.

(12) Lu, X.; Elimelech, M. Fabrication of desalination membranes by interfacial polymerization: history, current efforts, and future directions. *Chem. Soc. Rev.* **2021**,

(13) Li, Y.; Li, Z.; Aydin, F.; Quan, J.; Chen, X.; Yao, Y.-C.; Zhan, C.; Chen, Y.; Pham, T. A.; Noy, A. Water-ion permselectivity of narrow-diameter carbon nanotubes. *Sci. Adv.* **2020**, *6*, eaba9966.

(14) Freger, V. Selectivity and polarization in water channel membranes: lessons learned from polymeric membranes and CNTs. *Faraday Discuss.* **2018**, *209*, 371–388.

(15) Amiri, H.; Shepard, K. L.; Nuckolls, C. R. l. Hernández Sánchez. *Nano Lett.* **2017**, *17*, 1204–1211.

(16) Corry, B. Designing carbon nanotube membranes for efficient water desalination. *J. Phys. Chem. B* **2008**, *112*, 1427–1434.

(17) Song, C.; Corry, B. Intrinsic ion selectivity of narrow hydrophobic pores. *J. Phys. Chem. B* **2009**, *113*, 7642–7649.

(18) Hummer, G.; Rasaiah, J. C.; Noworyta, J. P. Water conduction through the hydrophobic channel of a carbon nanotube. *Nature* **2001**, *414*, 188–190.

(19) Striolo, A. The mechanism of water diffusion in narrow carbon nanotubes. *Nano Lett.* **2006**, *6*, 633–639.

(20) Won, C. Y.; Joseph, S.; Aluru, N. Effect of quantum partial charges on the structure and dynamics of water in single-walled carbon nanotubes. *J. Chem. Phys.* **2006**, *125*, 114701.

(21) Chaban, V. V.; Prezhdo, V. V.; Prezhdo, O. V. Confinement by carbon nanotubes drastically alters the boiling and critical behavior of water droplets. *ACS Nano* **2012**, *6*, 2766–2773.

(22) Falk, K.; Sedlmeier, F.; Joly, L.; Netz, R. R.; Bocquet, L. Molecular origin of fast water transport in carbon nanotube membranes: superlubricity versus curvature dependent friction. *Nano Lett.* **2010**, *10*, 4067–4073.

(23) Liu, L.; Patey, G. Simulated conduction rates of water through a (6, 6) carbon nanotube strongly depend on bulk properties of the model employed. *J. Chem. Phys.* **2016**, *144*, 184502.

(24) Samoylova, O. N.; Calixte, E. I.; Shuford, K. L. Molecular dynamics simulations of ion transport in carbon nanotube channels. *J. Phys. Chem. C* **2015**, *119*, 1659–1666.

(25) Tunuguntla, R. H.; Henley, R. Y.; Yao, Y.-C.; Pham, T. A.; Wanunu, M.; Noy, A. Enhanced water permeability and tunable ion selectivity in subnanometer carbon nanotube porins. *Science* **2017**, *357*, 792–796.

(26) Tunuguntla, R. H.; Allen, F. I.; Kim, K.; Belliveau, A.; Noy, A. Ultrafast proton transport in sub-1-nm diameter carbon nanotube porins. *Nat. Nanotechnol* **2016**, *11*, 639–644.

(27) Secchi, E.; Niguès, A.; Jubin, L.; Siria, A.; Bocquet, L. Scaling behavior for ionic transport and its fluctuations in individual carbon nanotubes. *Phys. Rev. Lett.* **2016**, *116*, 154501.

(28) Majumder, M.; Chopra, N.; Andrews, R.; Hinds, B. J. Enhanced flow in carbon nanotubes. *Nature* **2005**, *438*, 44–44.

(29) Miller, S. A.; Young, V. Y.; Martin, C. R. Electroosmotic flow in template-prepared carbon nanotube membranes. *J. Am. Chem. Soc.* **2001**, *123*, 12335–12342.

(30) Kalra, A.; Garde, S.; Hummer, G. Osmotic water transport through carbon nanotube membranes. *PNAS* **2003**, *100*, 10175–10180.

(31) Keerthi, A.; Geim, A.; Janardanan, A.; Rooney, A.; Esfandiar, A.; Hu, S.; Dar, S.; Grigorieva, I.; Haigh, S.; Wang, F., et al. Ballistic molecular transport through two-dimensional channels. *Nature* **2018**, *558*, 420–424.

(32) Hong, Y.; Zhang, J.; Zhu, C.; Zeng, X. C.; Francisco, J. S. Water desalination through rim functionalized carbon nanotubes. *J. Mater. Chem. A* **2019**, *7*, 3583–3591.

(33) Hou, Y.; Wang, M.; Chen, X.; Hou, X. Continuous water-water hydrogen bonding network across the rim of carbon nanotubes facilitating water transport for desalination. *Nano Res.* **2021**, 1–8.

(34) Corry, B. Water and ion transport through functionalised carbon nanotubes: implications for desalination technology. *Energy Environ. Sci.* **2011**, *4*, 751–759.

(35) Biesheuvel, P.; Bazant, M. Analysis of ionic conductance of carbon nanotubes. *Phys. Rev. E* **2016**, *94*, 050601.

(36) Uematsu, Y.; Netz, R. R.; Bocquet, L.; Bonthuis, D. J. Crossover of the power-law exponent for carbon nanotube conductivity as a function of salinity. *J. Phys. Chem. B* **2018**, *122*, 2992–2997.

(37) Kavokine, N.; Netz, R. R.; Bocquet, L. Fluids at the nanoscale: From continuum to subcontinuum transport. *Annu. Rev. Fluid Mech.* **2021**, *53*, 377–410.

(38) Noh, Y.; Aluru, N. R. Ion transport in electrically imperfect nanopores. *ACS Nano* **2020**, *14*, 10518–10526.

(39) Sarkadi, Z.; Fertig, D.; Ható, Z.; Valiskó, M.; Boda, D. From nanotubes to nanoholes: Scaling of selectivity in uniformly charged nanopores through the Dukhin number for 1: 1 electrolytes. *J. Chem. Phys.* **2021**, *154*, 154704.

(40) Yao, Y.-C.; Taqieddin, A.; Alibakhshi, M. A.; Wanunu, M.; Aluru, N. R.; Noy, A. Strong electroosmotic coupling dominates ion conductance of 1.5 nm diameter carbon nanotube porins. *ACS Nano* **2019**, *13*, 12851–12859.

(41) Manghi, M.; Palmeri, J.; Yazda, K.; Henn, F.; Jourdain, V. Role of charge regulation and flow slip in the ionic conductance of nanopores: An analytical approach. *Phys. Rev. E* **2018**, *98*, 012605.

(42) Gao, X. *Molecular Dynamics Study of Water and Ion Transport in Carbon Nanotubes and Slit Nanochannels*; Hong Kong University of Science and Technology (Hong Kong), 2017.

(43) Beu, T. A. Molecular dynamics simulations of ion transport through carbon nanotubes. I. Influence of geometry, ion specificity, and many-body interactions. *J. Chem. Phys.* **2010**, *132*, 164513.

(44) Beu, T. A. Molecular dynamics simulations of ion transport through carbon nanotubes.

II. Structural effects of the nanotube radius, solute concentration, and applied electric fields. *J. Chem. Phys.* **2011**, *135*, 044515.

(45) Ailenei, A.-E.; Beu, T. A. Ion transport through gated carbon nanotubes: molecular dynamics simulations using polarizable water. *J. Mol. Struct.* **2021**, 131022.

(46) Li, Z.; Li, Y.; Yao, Y.-C.; Aydin, F.; Zhan, C.; Chen, Y.; Elimelech, M.; Pham, T. A.; Noy, A. Strong Differential Monovalent Anion Selectivity in Narrow Diameter Carbon Nanotube Porins. *ACS Nano* **2020**, *14*, 6269–6275.

(47) Neklyudov, V.; Freger, V. Water and Ion Transfer to Narrow Carbon Nanotubes: Roles of Exterior and Interior. *J. Phys. Chem. Lett.* **2020**, *12*, 185–190.

(48) Grosjean, B.; Pean, C.; Siria, A.; Bocquet, L.; Vuilleumier, R.; Bocquet, M.-L. Chemisorption of hydroxide on 2D materials from DFT calculations: graphene versus hexagonal boron nitride. *J. Phys. Chem. Lett.* **2016**, *7*, 4695–4700.

(49) Beckstein, O.; Sansom, M. S. The influence of geometry, surface character, and flexibility on the permeation of ions and water through biological pores. *Phys. Biol.* **2004**, *1*, 42.

(50) Waghe, A.; Rasaiah, J. C.; Hummer, G. Entropy of single-file water in (6, 6) carbon nanotubes. *J. Chem. Phys.* **2012**, *137*, 044709.

(51) Agrawal, K. V.; Shimizu, S.; Drahushuk, L. W.; Kilcoyne, D.; Strano, M. S. Observation of extreme phase transition temperatures of water confined inside isolated carbon nanotubes. *Nat. Nanotechnol* **2017**, *12*, 267–273.

(52) Zhan, C.; Aydin, F.; Schwegler, E.; Noy, A.; Pham, T. A. Understanding Cation Selectivity in Carbon Nanopores with Hybrid First-Principles/Continuum Simulations: Implications for Water Desalination and Separation Technologies. *ACS Appl. Nano Mater.* **2020**, *3*, 9740–9748.

(53) Dilger, J. P.; McLaughlin, S.; McIntosh, T. J.; Simon, S. A. The dielectric constant of phospholipid bilayers and the permeability of membranes to ions. *Science* **1979**, *206*, 1196–1198.

(54) Aydin, F.; Moradzadeh, A.; Bilodeau, C. L.; Lau, E. Y.; Schwegler, E.; Aluru, N. R.; Pham, T. A. Ion Solvation and Transport in Narrow Carbon Nanotubes: Effects of Polarizability, Cation- $\pi$ Interaction, and Confinement. *J. Chem. Theory Comput.* **2021**, *17*, 1596–1605.

(55) Levy, A.; de Souza, J. P.; Bazant, M. Z. Breakdown of electroneutrality in nanopores. *J. Colloid Interface Sci.* **2020**, *579*, 162–176.

(56) Lee, S. H.; Rasaiah, J. C. Proton transfer and the diffusion of H+ and OH- ions along water wires. *J. Chem. Phys.* **2013**, *139*, 124507.

(57) Dellago, C.; Naor, M. M.; Hummer, G. Proton transport through water-filled carbon nanotubes. *Phys. Rev. Lett.* **2003**, *90*, 105902.

(58) Grosjean, B.; Bocquet, M.-L.; Vuilleumier, R. Versatile electrification of two-dimensional nanomaterials in water. *Nat. Commun.* **2019**, *10*, 1–8.

(59) Freger, V. Ion partitioning and permeation in charged low-T* membranes. *Adv. Colloid Interface Sci.* **2020**, *277*, 102107.

(60) Schienbein, P.; Schwaab, G.; Forbert, H.; Havenith, M.; Marx, D. Correlations in the solute–solvent dynamics reach beyond the first hydration shell of ions. *J. Phys. Chem. Lett.* **2017**, *8*, 2373–2380.

(61) Balos, V.; Imoto, S.; Netz, R. R.; Bonn, M.; Bonthuis, D. J.; Nagata, Y.; Hunger, J. Macroscopic conductivity of aqueous electrolyte solutions scales with ultrafast microscopic ion motions. *Nat. Commun.* **2020**, *11*, 1–8.

(62) Gillan, M.; Alfe, D. and A. Michaelides. *J. Chem. Phys* **2016**, *144*, 130901.

(63) Li, F.; Wang, L.; Zhao, J.; Xie, J. R.-H.; Riley, K. E.; Chen, Z. What is the best density functional to describe water clusters: Evaluation of widely used density functionals with various basis sets for $(H_2O)_n$ (n = 1-10). *Theor. Chem. Acc.* **2011**, *130*, 341–352.

(64) Temelso, B.; Archer, K. A.; Shields, G. C. Benchmark structures and binding energies of small water clusters with anharmonicity corrections. *J. Phys. Chem. A* **2011**, *115*, 12034–12046.

(65) Mejıas, J.; Lago, S. Calculation of the absolute hydration enthalpy and free energy of H+ and OH-. *J. Chem. Phys.* **2000**, *113*, 7306–7316.

(66) Śmiechowski, M.; Stangret, J. Hydroxide ion hydration in aqueous solutions. *J. Phys. Chem. A* **2007**, *111*, 2889–2897.

(67) Srinivasa Rao, J.; Dinadayalane, T.; Leszczynski, J.; Narahari Sastry, G. Comprehensive Study on the Solvation of Mono-and Divalent Metal Cations: Li+, Na+, K+, Be2+, Mg2+ and Ca. *J. Phys. Chem. A* **2008**, *112*, 12944–12953.

(68) Tobias, D. J.; Jungwirth, P.; Parrinello, M. Surface solvation of halogen anions in water clusters: An ab initio molecular dynamics study of the Cl-(H 2 O) 6 complex. *J. Chem. Phys.* **2001**, *114*, 7036–7044.

(69) Bajaj, P.; Riera, M.; Lin, J. K.; Mendoza Montijo, Y. E.; Gazca, J.; Paesani, F. Halide Ion Microhydration: Structure, Energetics, and Spectroscopy of Small Halide–Water Clusters. *J. Phys. Chem. A* **2019**, *123*, 2843–2852.

(70) Frisch, M. J. et al. *Gaussian 09 Revision B.01* **2009**,

(71) Chai, J.-D.; Head-Gordon, M. Long-range corrected hybrid density functionals with damped atom–atom dispersion corrections. *PCCP* **2008**, *10*, 6615–6620.

(72) Grimme, S.; Antony, J.; Ehrlich, S.; Krieg, H. A consistent and accurate ab initio

parametrization of density functional dispersion correction (DFT-D) for the 94 elements H-Pu. *J. Chem. Phys.* **2010**, *132*, 154104.

(73) Tomasi, J.; Mennucci, B.; Cammi, R. Quantum mechanical continuum solvation models. *Chem. Rev.* **2005**, *105*, 2999–3094.

(74) Laury, M. L.; Carlson, M. J.; Wilson, A. K. Vibrational frequency scale factors for density functional theory and the polarization consistent basis sets. *J. Comput. Chem.* **2012**, *33*, 2380–2387.

(75) Boys, S. F.; Bernardi, F. The calculation of small molecular interactions by the differences of separate total energies. Some procedures with reduced errors. *Mol. Phys.* **1970**, *19*, 553–566.

(76) Barone, V.; Cossi, M. Quantum calculation of molecular energies and energy gradients in solution by a conductor solvent model. *J. Phys. Chem. A* **1998**, *102*, 1995–2001.

(77) Cossi, M.; Scalmani, G.; Rega, N.; Barone, V. Energies, gradients, and harmonic frequencies for molecules in solution by the C-PCM solvation model. *J. Comput. Chem* **2003**, *24*, 669.

(78) Marcus, Y.; Ben Naim, A. Solvation dynamics of nonionic solutes. *J. Chem. Phys* **1984**, *81*, 2016–2027.

(79) Amicangelo, J. C.; Armentrout, P. Absolute binding energies of alkali-metal cation complexes with benzene determined by threshold collision-induced dissociation experiments and ab initio theory. *J. Phys. Chem. A* **2000**, *104*, 11420–11432.

(80) Courty, A.; Mons, M.; Dimicoli, I.; Piuzzi, F.; Gaigeot, M.-P.; Brenner, V.; de Pujo, P.; Millié, P. Quantum Effects in the Threshold Photoionization and Energetics of the Benzene- H2O and Benzene- D2O Complexes: Experiment and Simulation. *J. Phys. Chem. A* **1998**, *102*, 6590–6600.

(81) Ferretti, A.; Prampolini, G.; d'Ischia, M. Benchmarking Cation-$\pi$ Interactions: Assessment of DFT and Moeller-Plesset Second Order Perturbation Theory Calculations with Optimized Basis Sets (MP2mod) for Complexes of Benzene, Phenol and Catechol with Na+, K+, Rb+ and Cs. *J. Phys. Chem. A* **2020**,

(82) Upadhyay, D.; Mishra, P. Binding of benzene with water clusters (H2O) n, n= 1–6, in the ground and lowest singlet excited states. *J. Mol. Struct.: THEOCHEM* **2002**, *584*, 113–133.

(83) Ma, J.; Alfè, D.; Michaelides, A.; Wang, E. The water-benzene interaction: Insight from electronic structure theories. *J. Chem. Phys.* **2009**, *130*, 154303.

(84) Schyman, P.; Jorgensen, W. L. Exploring adsorption of water and ions on carbon surfaces using a polarizable force field. *J. Phys. Chem. Lett.* **2013**, *4*, 468–474.

(85) Wheeler, S. E.; Houk, K. Are Anion/$\pi$ Interactions Actually a Case of Simple Charge-Dipole Interactions? *J. Phys. Chem. A* **2010**, *114*, 8658–8664.

(86) Lucas, X.; Quinonero, D.; Frontera, A.; Deya, P. M. Counterintuitive Substituent Effect of the Ethynyl Group in Ion- $\pi$ Interactions. *J. Phys. Chem. A* **2009**, *113*, 10367–10375.

(87) Vlcek, L.; Chialvo, A. A. Single-ion hydration thermodynamics from clusters to bulk solutions: Recent insights from molecular modeling. *Fluid Ph. Equilibria* **2016**, *407*, 58–75.